

The importance of ice sheet growth and retreat on magmatism and mantle CO₂ flux

John J. Armitage¹, David J. Ferguson², Kenni D. Petersen³, and Timothy T. Creyts⁴

¹Dynamique des Fluides Géologiques, Institut de Physique du Globe de Paris, Paris, France

²School of Earth and Environment, University of Leeds, Leeds, U.K.

³Department of Geoscience, University of Aarhus, Aarhus, Denmark

⁴Lamont-Doherty Earth Observatory, Columbia University, U.S.A

Key Points:

- We combine a new history of Icelandic ice-cover with a forward model of magma generation.
- Magmatism and CO₂ outgassing is influenced by both the rate of deglaciation and, importantly, the preceding growth of the ice sheet.
- Something about the interplay between ice sheets and CO₂

15 **Abstract**

16 Climate cycles may significantly affect the eruptive behavior of terrestrial volcanoes due
 17 to pressure changes caused by glacial loading, which raises the possibility that climate
 18 change may modulate CO₂ degassing via volcanism. In Iceland, magmatism is likely to
 19 have been influenced by glacial activity. To explore if deglaciation therefore impacted
 20 CO₂ flux we coupled a model of glacial loading over the last ~120 ka to melt generation
 21 and transport. We find that a nuanced relationship exists between magmatism and glacial
 22 activity. Enhanced CO₂ degassing happened prior to the main phase of late-Pleistocene
 23 deglaciation, and it is sensitive to the duration of the growth of the ice sheet entering
 24 into the LGM, as well as the rate of ice loss. Ice sheet growth depresses melting in the
 25 upper mantle, creating a delayed pulse of CO₂ out-gassing as the magmatic system re-
 26 covers from the effects of loading.

27 **1 Introduction**

28 Evidence from several tectonic settings indicates that glaciated volcanic systems
 29 respond to changing ice volumes (Glazner, Manley, Marron, & Rojstaczer, 1999; Jellinek,
 30 Mange, & Saar, 2004; Jull & McKenzie, 1996; MacLennan, Jull, McKenzie, Slater, & Grönvöld,
 31 2002; Rawson et al., 2016; Sigvaldson, Annertz, & Nilsson, 1992), and suggests there was
 32 a widespread volcanic response to late-Pleistocene ice retreat (Huybers & Langmuir, 2009).
 33 The most compelling evidence for climate-coupled volcanism comes from Iceland, where
 34 changes in early Holocene lava volumes and magma chemistry are consistent with de-
 35 pressurization during glacial unloading (Jull & McKenzie, 1996; MacLennan et al., 2002;
 36 Sinton, Grönvöld, & Saemundsson, 2005). Magma generation here occurs due to pressure-
 37 release melting, as the mantle up-wells beneath rift zones. Although the net change in
 38 overburden pressures from variations in ice cover red have been relatively small, the high
 39 rates of change associated with glacial activity can produce significant short-term fluc-
 40 tuations in magmatic output (Jull & McKenzie, 1996; ?; ?), similar to those hypoth-
 41 esised to occur at ocean ridges due to sea-level variation (Burley & Katz, 2015; Crowley,
 42 Katz, Huybers, Langmuir, & Park, 2015; Huybers & Langmuir, 2009; Lund & Asimow,
 43 2011). Carbon readily partitions into magmas during partial melting (Rosenthal, Hauri,
 44 & Hirschmann, 2015) and is released as a CO₂ rich fluid/vapour as the magma ascends
 45 through the crust, making volcanism the primary pathway for transporting carbon from
 46 the Earth's mantle to the atmosphere (Dasgupta & Hirschmann, 2010). However, car-
 47 bon does not enter the melt uniformly during partial melting and is concentrated in early
 48 formed magma and does not enter the melt uniformly over time. Therefore the extent
 49 to which glacially driven changes in primary magma generation alter the flux of CO₂ de-
 50 pends on where in the melting column melt production is enhanced (or suppressed), the
 51 rate of melt transport, and the history of ice sheet growth and retreat.

52 Global data sets of the number of volcanic eruptions throughout the Pleistocene
 53 would suggest there is a correlation between climatic change and volcanism (Huybers
 54 & Langmuir, 2009), yet data resolution makes testing this association difficult. It is thought
 55 that CO₂ and the trace element Nb have a relatively similar behaviour during decom-
 56 pression melting (?), and as such Nb compositions can be used to gauge the quantity
 57 of CO₂ erupted. In Iceland there are just over 300 published dated analysis of the Nb
 58 composition of Pleistocene lavas (Gee, Taylor, Thirwall, & Murton, 1998; ?). This is ar-
 59 guably the most complete geochemical record within a region that experienced signif-
 60 icant Pleistocene deglaciation. In this study we take a new approach, and use a high res-
 61 olution model of ice sheet history to drive a forward model of melt generation and trans-
 62 port. We predict the change in eruption rates and melt composition as a function of the
 63 changing surface load, and also validate the predicted melt porosity against the seismic
 64 structure imaged below Iceland. We subsequently explore under what conditions climate
 65 and magmatism might be related, and the implications for CO₂ degassing.

66 **2 Methods**

67 **2.1 Modelling of Melt Generation and Transport**

68 To investigate the impact of glacial activity on melt productivity, melt composition,
 69 and CO₂ flux, we used a model of magma generation and transport coupled to a
 70 model of the flexure of a viscoelastic beam for the response to change in load due to the
 71 ice sheet history (see Supplementary Material). The coupled model consists of a flexural
 72 model of the surface displacement due to the changing surface load as the ice sheet
 73 changes in thickness. This model of surface displacement is then coupled to either a 1D
 74 vertical column or a 2D corner flow model where the flow of the mantle is prescribed at
 75 either an upwelling rate of 10 or 20 mm yr⁻¹, or lateral spreading rate of 10 mm yr⁻¹. We
 76 use these two upwelling rates to cover the uncertainty in the exact rate of vertical as-
 77 cent the mantle below Iceland due to mantle buoyancy. The upwelling column is per-
 78 turbed by the displacement due to loading, where the viscoelastic decay time of the load
 79 is set to 1000 yrs. Carbon partitioning into the melt is assumed to be governed by the
 80 coefficients derived by (Rosenthal et al., 2015). We use a mantle source composition for
 81 Nb of 1.627 ppm, which is intermediate between the end-member sources for Icelandic
 82 melts identified by (Shorttle & MacLennan, 2011). To approximate the melting of the mul-
 83 tiple source lithologies we chose a solidus-depletion gradient of 600 °C which is interme-
 84 diate between that of melting experiments on depleted mantle, 900 °C (Wasylewski, Baker,
 85 Kent, & Stopler, 2003) and fertile mantle 300 °C (Scott, 1992).

86 The surface expression of partial melting to glacial loading/unloading is influenced
 87 primarily by the rate at which the melt percolates through the mantle (Burley & Katz,
 88 2015). To constrain the permeability of melt transport, we examined the effects of vary-
 89 ing the permeability coefficient on the seismic properties of the mantle produced by our
 90 1-D model. The thermal structure and porosity was converted to S-wave velocities, as-
 91 suming that melt reduces the velocity by 7.9 % per percent porosity (Hammond & Humphreys,
 92 2000) and including the effects of attenuation (Goes, Armitage, Harmon, Huismans, &
 93 Smith, 2012). Recent joint inversion of teleseismic and ambient noise Rayleigh waves in
 94 Iceland would suggest that the S-wave velocity is between 4 and 3.8 km s⁻¹ at depths
 95 of 50 to 150 km (Harmon & Rychert, 2016) (Figure 1). We find that the permeability
 96 coefficient, k_0 , needs to be relatively high (10^{-5} m²) giving a permeability, $k_\phi = k_0 \phi^3$
 97 (where ϕ is porosity), of the order of 10^{-14} m² ($\phi \approx 0.001$; Figure 1), because other-
 98 wise porosity would be too large and the S-wave velocity would decrease below the ob-
 99 served values. This permeability is an order of magnitude higher than the upper range
 100 used to explore how sea-level change might influence mid-ocean ridge (MOR) magma-
 101 tism (Burley & Katz, 2015; Crowley et al., 2015), and suggests rates of magmatic ascent
 102 of the order of 10 m yr⁻¹, in agreement with MacLennan et al. (2002). Previously it has
 103 been suggested that delays in signal propagation from the zone of partial melting at MORs
 104 to the surface might be of the order of a Milankovitch-scale period, 40 kyr (Huybers &
 105 Langmuir, 2017). However, the high permeability required to match the seismic obser-
 106 vations from Iceland implies a magmatic system that much more rapidly responds to change
 107 in melting conditions, consistent with the fast transport rates estimated from U-series
 108 isotope studies (Elliot & Spiegelman, 2014).

109 **2.2 Glacial Forcing Throughout the Pleistocene**

110 Iceland experienced extensive ice-cover during the last glacial period (Patton, Hub-
 111 bard, Bradwell, & Schomackere, 2017), with maximum thicknesses in the center of the
 112 island of ~ 2km attained by ~23 ka (Figure 2a and b). Deglaciation after the LGM oc-
 113 curred at a varying rate, and was discontinuous. For example, a stage of re-advance oc-
 114 curred during the colder climate of the Younger Dryas (11.7-12.9 ka) (Nordahl & Ingólfsson,
 115 2015). The final phase of deglaciation was particularly rapid, with the main volcanic zones
 116 being largely ice free by ~10 ka (Figure 2a). The most uncertain period of the glacial

history is the pre-LGM growth of the ice sheet. To create the ice sheet histories shown in Figure 2b and Figure 3a we calibrated the ice volume since the LGM against the North Greenland Ice Core Project (NGRIP) $\delta^{18}\text{O}$ record, and Quaternary sea-level curves assuming a linear correlation between these three signals (see Supplementary Material Text S1). We focus on two scenarios: M1, based on the ICE-5G sea-level curves (Peltier, 2004), and M2, based on the sea-level curves of Pico, Creveling, and Mitrovica (2017) (Figure S2).

3 Results

We force our melt model with the 120 ka glacial history after a 5 Myr model wind-up to steady state (model M1, Figure 2b) and using a single value for the ice thickness at each time-step, therefore neglecting the effects of the distal parts of the ice sheet on melting beneath the rift margins. The model predicts peaks in magmatic output and CO_2 flux as pressure changes due to loading and unloading impact the melt production rate (Figure 2). The response of the magmatic system to changes in ice cover varies depending on the mantle upwelling rate, the rate-of-change in ice sheet thickness, and the prior ice sheet history. Glacial loading suppresses melt production, leading to a decline in magma supply (see Supplementary Material, Figure S3). For example during the period between 35 and 15 ka, the growth of the ice sheet reduces eruption rates below 5 km of melt per Myr (Figure 2c). The recovery from this loading occurs initially in the deepest part of the system as this region is perturbed the least. Recovery is also faster if the mantle upwelling rate is higher, where an upwelling rate of 20 mm yr^{-1} is more responsive than the equivalent 10 mm yr^{-1} model (Figure 2b). Higher rates of change in surface loading will impact melt production more strongly such that small magnitude but rapid deglaciation events, for example at ~ 85 ka, have a relatively large effect on eruption rates (Figure 2c).

The impact of deglaciation events is modulated by the upwelling rate of the solid mantle because the upwelling rate controls the background productivity of the melting model. At slower upwelling rates, i.e. 10 mm yr^{-1} , some periods of deglaciation are not recorded in the flux of magma erupted. An example of this is the warming event at 60 ka (Figure 2), where the 10 mm yr^{-1} upwelling model produces no response in either the eruption rate or CO_2 flux. If however upwelling is more rapid, 20 mm yr^{-1} , then there is a clear pulse in melt eruption rate (Figure 2). This is because porosity and productivity are so low, that any pulse in melt production does not reach the surface.

Our models indicate that deglaciation-enhanced melt productivity is not only a function of the rate of deglaciation, but is strongly dependent on the preceding glacial history. For example, in the 20 mm yr^{-1} upwelling rate model, the largest CO_2 peak is estimated to occur at ~ 60 ka and not during the volumetrically larger magmatic pulse at the end of the Pleistocene (Figure 2d). This difference is because when the ~ 60 ka warming occurred, the melt was enriched in carbon due to the preceding rapid glaciation. Magma supplied from the mantle during the Late-Pleistocene pulse were more depleted in carbon compared to those in the 60 ka event.

4 Glacial Forcing Through the Latest Pleistocene and Holocene

There are two distinct late Pleistocene magmatic pulses, separated by the Younger Dryas cold period (Figure 3a and b). However, for the model M2 ice sheet history there are three pulses in CO_2 flux at the end of the Pleistocene, due to the faster ice sheet growth entering the LGM from 35 to 25 ka in this model (Figure 3a and e). This peak in CO_2 flux is because the small magnitude but rapid deglaciations after 25 ka tap melts rich in trace elements including Nb and carbon (Figure 3c and d).

The observed time series of incompatible trace element concentrations in Icelandic magmas and ice sheet history have been suggested to be strongly associated (Eason, Sin-

ton, Gronvöld, & Kurz, 2015; Gee et al., 1998; Jull & McKenzie, 1996; Maclennan et al., 2002; Sinton et al., 2005). Of these studies Gee et al. (1998) and Eason et al. (2015) report on the Nb composition of lavas erupted and give age ranges for the erupted lavas. Dating lava flow in Iceland is complex given the lack of reliable markers from which ages can be obtained. This means that ages are instead typically taken from the stratigraphy and visual correlations between erupted flows (Maclellan et al., 2002). We therefore must take the age ranges for the Nb compositions reported by Gee et al. (1998) and citeeason-etal-2015 as indicative and not absolute. We therefore chose to bin the ages into 2.5 kyr intervals from 0 to 17.5 ka and then at 5 kyr intervals (Figure 3c). The reduction in Nb compositions plotted is in line with the more selective La and Sm data set presented in Maclellan et al. (2002), and is therefore likely robust.

We find that the predicted change in Nb, which behaves in a similar way to C during mantle melting (Rosenthal et al., 2015), from all our models fit within the range of the observations (Figure 3c). The M2 model gives the strongest signature in Nb concentrations of deglaciation during the end of the Pleistocene, while the signature is more subdued in the M1 ice sheet model (Figure 3c). The 1D forward model used is highly idealised, and yet the agreement between the observations and model is encouraging, and suggests the compositional change observed in lavas erupted during the late-Pleistocene to early Holocene is due to rapid deglaciation (Eason et al., 2015; Gee et al., 1998; Maclellan et al., 2002; Sinton et al., 2005). This implies that the observed change in melt composition is due to change in ice sheet loading and that the pre-deglaciation volcanism likely released a significant volume of CO₂ (Figure 3e).

The 1D column model will underestimate the impact of change in deep melt productivity, as it cannot capture the deep wings of the zone of partial melting. To explore the impact of this we force a series of 1D models with the vertical flow taken from steady state corner flow perturbed by the flexural response of the deglaciation of a 200 km wide ice sheet. The half spreading rate is assumed to be 10 mm yr⁻¹, and the mantle potential temperature is 1450 °C. Melt travels vertically from the zone of partial melting in columns at 0 to 80 km from the rift axis (Figure 4). The steady state thickness of melt erupted at the surface of the simplified 2D model is 15 km, and glacial forcing causes this thickness to vary around this value by the order of 10 km except for a large spike at the LGM (Figure NEW). The crust of Iceland varies in thickness from 20 to 40 km (?), and therefore a model steady state thickness of 15 km is a reasonable lower end-member prediction given that the crust is made of extrusions and intrusions.

After glacial perturbation we find that in the central zone, from the ridge centre to 40 km distance, the trend in Nb and CO₂ flux is relatively similar, with a reduction in Nb at 15 ka. At distances greater than 40 km, a peak in Nb and CO₂ flux is predicted to occur with an increasing delay compared to the centre of extension (Figure 4). This delay is due to the greater distance that the melt has to travel along the vertical path from the top of the melt zone to the surface at increasing distance from the centre of extension. In full 2D models the distal melt will pool as it migrates laterally towards the centre of extension (Katz, 2008), yet the difference in ascent velocity due to the increase porosity as the melt pools would likely not be sufficient to overcome the increased distance that the signal will have to travel.

The full solution to the coupled equations of magma dynamics would suggest that melts generated at a distance of up to 60 km from the centre of extension are advected to the ridge axis (Katz, 2008). If all of the melt generated up to 60 km from the centre of extension is erupted, then the CO₂ flux is significantly increased during the Holocene due to the addition input of melt from the distal parts of the zone of partial melting (Figure 4b). Therefore these low productivity and deep regions of the zone of partial melting might be a key exporter of mantle carbon into the atmosphere. However, the range of observed Nb concentrations are relatively similar to the axial concentrations, from within <40 km of the rift centre (Figure 4). This would suggest that the widest regions of the

219 zone of partial melting are not sampled by the volcanism in the Reykjanes Ridge and
 220 Western Volcanic Zone, leading to an estimate of CO₂ fluxes more in line with the sim-
 221 pler 1D model.

222 5 Discussion and Conclusions

223 The models imply that the deglaciation beginning at 18 ka and continuing through
 224 the Bolling warming at 14.8 ka released substantial quantities of CO₂ when compared
 225 to the last 120 ka (Figure 3c and Figure 4b), and this elevated CO₂ release was because
 226 of the preceding growth of the ice sheet. Volcanism during this time would have taken
 227 place in a sub-glacial environment and unsurprisingly does not feature in the post-glacial
 228 sub-aerial record. Evidence from sub-glacial volcanic units (tuyas) erupted during this
 229 time period (Hartley, Thordarson, & de Joux, 2016) suggest volumetric and composi-
 230 tional trends consistent with those predicted by our model (Figure 3c and Figure 4).

231 Forcing our model with the long-term 120 ka ice sheet history produces a periodic
 232 fluxing of CO₂ from Icelandic volcanoes due to ice-loss events over this period, implying
 233 a close link between ice dynamics and magmatic out-gassing. The greatest release
 234 of CO₂, however, occurred during the period of ice-loss just before the Younger Dryas
 235 (~14 ka), and therefore before the largest phase of late-Pleistocene deglaciation (Figure
 236 4). The concentration of CO₂ released in this magmatic pulse was enhanced due to the
 237 lack of any significant loss of ice volume since ~40 ka. This created a magmatic system
 238 capable of fluxing large volumes of carbon during the initial period of post-LGM deglacia-
 239 tion (both models M1 and M2, Figure 3e), possibly contributing to the increased atmo-
 240 spheric CO₂ levels thought to be recorded between 15 and 14 ka in the EPICA Dome C
 241 ice core (Köhler, Knorr, Buiron, Lourantou, & Chappellaz, 2011). It is therefore possi-
 242 ble that this pulse of magmagenic CO₂, from Iceland and elsewhere (e.g. /citephuybers-
 243 2009, bolstered the climate warming, and final phase of deglaciation, that proceeded the
 244 Younger Dryas.

245 The CO₂ flux due to deglaciation is strongly influenced by the prior ice sheet growth.
 246 It is the sustained growth of the Icelandic ice sheet before 25 ka lead to the significant
 247 pulse in volcanism and CO₂ upon deglaciation at the end of the Pleistocene (Figure 4).
 248 This would imply that while a rapid loss of mass can trigger increased eruptions, the im-
 249 pact on atmospheric CO₂ concentrations is strongly modulated by the full history of the
 250 changing surface load. In effect we cannot conclude that all deglaciation events, or other
 251 rapid unloading events due to for example erosion, lead to a large flux of volatile gases
 252 into the Earths atmosphere. The Earth system is more complex than such simple causal-
 253 ity, yet one clear implication is that deglaciation after a prolonged period of ice-house
 254 conditions will lead to a significant carbon degassing of the upper mantle.

255 Supporting Information

256 A detailed discussion of the methodology can be found in the supporting informa-
 257 tion (Andersen et al., 2004; Andrews, 2008; Armitage, Collier, Minshull, & Henstock, 2011;
 258 Clark et al., 2009; Geirsdóttir, 2011; Gibson & Geist, 2010; Gureenko & Chaussidon, 1995;
 259 Katz, Spiegelman, & Langmuir, 2003; Lambeck & Chappel, 2001; Lambeck, Rouby, Pur-
 260 cell, Sun, & Sambridge, 2014; McKenzie & O’Nions, 1991; Miller, Zhu, Montési, & Gae-
 261 tani, 2014; Ribe, 1985; Scott, 1992; Shorttle & MacLennan, 2011; Silbeck, 1975; Sleep &
 262 Snell, 1976; Spiegelman, 1996; Spratt & Lisicki, 2016).

263 Acknowledgments

264 We would like to thank M. A. Mary Gee (The University of Western Australia) for shar-
 265 ing her Nb composition data from the Reykjanes Peninsula, and Tamara Pico (Harvard
 266 University) for sharing her sea level curves. John J. Armitage acknowledges funding from

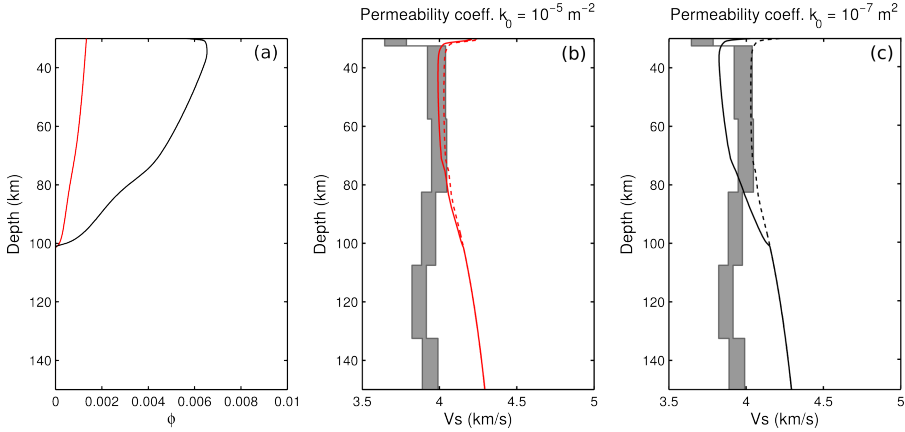
267 an Agence National de la Recherche (France), Accueil de Chercheurs de Haute Niveau,
 268 grant InterRift. The 1-D melting model is available from <https://bitbucket.com/johnjarmitage/melt1d-icesheet/>
 269

270 **References**

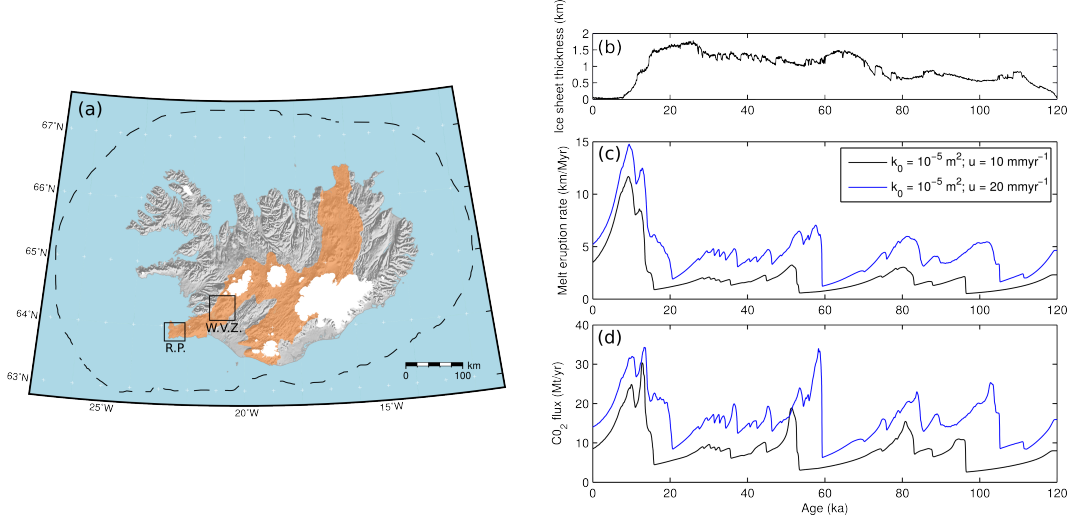
- 271 Andersen, K. K., Azuma, N., Barnola, J. M., Bigler, M., Biscaye, P., Caillon, N.,
 272 ... White, J. W. C. (2004). High-resolution record of northern hemisphere
 273 climate extending into the last interglacial period. *Nature*, *431*, 174-151. (doi:
 274 10.1038/nature02805)
- 275 Andrews, J. T. (2008). The role of the Iceland Ice Sheet in the North Atlantic dur-
 276 ing the late Quaternary: a review and evidence from Denmark Strait. *Journal*
 277 *of Quaternary Science*, *23*, 3-20. (doi: 10.1002/jqs.1142)
- 278 Armitage, J. J., Collier, J. S., Minshull, T. A., & Henstock, T. J. (2011). Thin
 279 oceanic crust and flood basalts: India-Seychelles breakup. *Geochemistry Geo-*
 280 *physics Geosystems*, *12*(Q0AB07). (doi:10.1029/2010GC003316)
- 281 Burley, J. M. A., & Katz, R. F. (2015). Variations in mid-ocean ridge CO₂ emis-
 282 sions driven by glacial cycles. *Earth and Planetary Science Letters*, *426*, 246-
 283 258. (doi: 10.1016/j.epsl.2015.06.031)
- 284 Clark, P. U., Dyle, A. S., Shakun, J. D., Carlson, A. E., Clark, J., Wohlfarth, B., ...
 285 McCabe, A. M. (2009). The last glacial maximum. *Science*, *325*, 710. (doi:
 286 10.1126/science.1172873)
- 287 Crowley, J. W., Katz, R. F., Huybers, P., Langmuir, C. H., & Park, S. H. (2015).
 288 Glacial cycles drive variations in the production of oceanic crust. *Science*, *347*,
 289 1237-1240. (doi: 10.1126/science.1261508)
- 290 Dasgupta, R., & Hirschmann, M. M. (2010). The deep carbon cycle and melting
 291 in Earth's interior. *Earth and Planetary Science Letters*, *298*, 1-13. (doi:
 292 10.1016/j.epsl.2010.06.039)
- 293 Eason, D. E., Sinton, J. M., Gronvöld, K., & Kurz, M. D. (2015). Effects of
 294 deglaciation on the petrology and eruptive history of the Western Volcanic
 295 Zone, Iceland. *Bulletin of Volcanology*, *77*(47). (doi: 10.1007/s00445-015-0916-
 296 0)
- 297 Elliot, T., & Spiegelman, M. (2014). Melt migration in oceanic crustal production:
 298 A u-series perspective. In *Treatise on geochemistry* (2nd ed., p. 543-581). Else-
 299 vier. (doi: 10.1016/B978-0-08-095975-7.00317-X)
- 300 Gee, M. A. M., Taylor, R. N., Thirwall, M., & Murton, B. J. (1998). Glacioisostacy
 301 controls chemical and isotopic characteristics of tholeiites from the Reykjanes
 302 Peninsula, SW Iceland. *Earth and Planetary Science Letters*, *164*, 1-5.
- 303 Geirsdóttir, A. (2011). Pliocene and pleistocene glaciations of iceland: a brief
 304 overview of the glacial history. In J. Ehlers, P. L. Gibbard, & P. Hughes
 305 (Eds.), *Quaternary glaciations - extent and chronology, a closer look* (Vol. 15,
 306 p. 199-210). Elsevier. (doi: 10.1016/B978-0-444-53447-7.00016-7)
- 307 Gibson, S. A., & Geist, D. (2010). Geochemical and geophysical estimates of litho-
 308 spheric thickness variation beneath galápagos. *Earth and Planetary Science*
 309 *Letters*, *300*, 275-286. (doi: 10.1016/j.epsl.2010.10.002)
- 310 Glazner, A. F., Manley, C. R., Marron, J. S., & Rojstaczer, S. (1999). Fire
 311 or ice: Anticorrelation of volcanism and glaciation in california over the
 312 past 800,000 years. *Geophysical Resaerch Letters*, *26*, 1759-1762. (doi:
 313 10.1029/1999GL900333)
- 314 Goes, S., Armitage, J. J., Harmon, N., Huismans, R., & Smith, H. (2012). Low seis-
 315 mic velocities below mid-ocean ridges: Attenuation vs. melt retention. *Journal*
 316 *of Geophysical Research*, *117*, B12403. (doi: 10.1029/2012JB009637)
- 317 Gurendo, A. A., & Chaussidon, M. (1995). Enriched and depleted primitive melts
 318 included in olivine from icelandic tholeiites: Origin by continuous melting of a
 319 single mantle column. *Geochimica et Cosmochimica Acta*, *59*, 2905-2917.

- 320 Hammond, W. C., & Humphreys, E. D. (2000). Upper mantle seismic wave ve-
 321 locity: Effects of realistic partial melt geometries. *Journal of Geophysical Re-*
 322 *search*, 105, 10975-10986.
- 323 Harmon, N., & Rychert, C. A. (2016). Joint inversion of teleseismic and ambient
 324 noise Rayleigh waves for phase velocity maps, an application to Iceland. *Jour-*
 325 *nal of Geophysical Research*, 121, 5966-5987. (doi: 10.1002/2016JB012934)
- 326 Hartley, M. E., Thordarson, T., & de Joux, A. (2016). Postglacial eruptive history
 327 of the Askja region, North Iceland. *Bulletin of Volcanology*, 78(28). (doi:
 328 10.1007/s00445-016-1022-7)
- 329 Huybers, P., & Langmuir, C. H. (2009). Feedback between deglacation, volca-
 330 nism, and atmospheric CO₂. *Earth and Planetary Science Letters*, 286, 479-491.
 331 (doi: 10.1016/j.epsl.2009.07.014)
- 332 Huybers, P., & Langmuir, C. H. (2017). Delayed CO₂ emissions from mid-ocean
 333 ridge volcanism as a possible cause of late-Pleistocene glacial cycles. *Earth and*
 334 *Planetary Science Letters*, 457, 238-249. (doi: 10.1016/j.epsl.2016.09.021)
- 335 Jellinek, M. A., Mange, M., & Saar, M. O. (2004). Did melting glaciers
 336 cause volcanic eruptions in eastern California? probing the mechanisms
 337 of dike formation. *Journal of Geophysical Research*, 109(B09206). (doi:
 338 10.1029/2004JB002978)
- 339 Jull, M., & McKenzie, D. (1996). The effect of deglaciation on mantle melting be-
 340 neath Iceland. *Journal of Geophysical Research*, 101(B10), 21815-21828.
- 341 Katz, R. F. (2008). Magma dynamics with the enthalpy method: Benchmark so-
 342 lutions and magmatic focusing at mid-ocean ridges. *Journal of Petrology*, 49,
 343 2099-2121. (doi:10.1093/petrology/egn058)
- 344 Katz, R. F., Spiegelman, M., & Langmuir, C. H. (2003). A new parameterization of
 345 hydrous mantle melting. *Geochemistry Geophysics Geosystems*, 4, 1073. (doi:
 346 10.1029/2002GC000433)
- 347 Köhler, P., Knorr, G., Buiron, D., Lourantou, A., & Chappellaz, J. (2011). Abrupt
 348 rise in atmospheric CO₂ at the onset of the Bolling/Allerod: in-situ ice core
 349 data versus true atmospheric signals. *Climate of the Past*, 7, 473-486. (doi:
 350 10.5194/cp-7-473-2011)
- 351 Kokfelt, T. F., Hoernle, K., & Hauff, F. (2003). Upwelling and melting of the Ice-
 352 land plume from radial variation of ²³⁸U - ²³⁰Th disequilibria in postglacial
 353 volcanic rocks. *Earth and Planetary Science Letters*, 214, 176-186. (doi:
 354 10.1016/S0012-821X(03)00306-6)
- 355 Lambeck, K., & Chappel, J. (2001). Sea level change through the last glacial cycles.
 356 *Science*, 292, 679-686. (doi: 10.1126/science.1059549)
- 357 Lambeck, K., Rouby, H., Purcell, A., Sun, Y., & Sambridge, M. (2014). Sea level
 358 and global ice volumes from the Last Glacial Maximum to the Holocene.
 359 *Proceedings of the National Academy of Sciences*, 111, 15296-15303. (doi:
 360 10.1073/pnas.141176211)
- 361 Lund, D. C., & Asimow, P. D. (2011). Does sea level influence mid-ocean ridge mag-
 362 matism on Milankovitch timescales? *Geochemistry Geophysics Geosystems*,
 363 12(Q12009). (doi: 10.1029/2011GC003693)
- 364 MacLennan, J., Jull, M., McKenzie, D., Slater, L., & Gronvöld, K. (2002). The
 365 link between volcanism and deglaciation in Iceland. *Geochemistry Geophysics*
 366 *Geosystems*, 3(11, 1062). (doi: 10.1029/2001GC000282)
- 367 MacLennan, J., McKenzie, D., & Gronvöld, K. (2001). Plume-driven upwelling un-
 368 der central Iceland. *Earth and Planetary Science Letters*, 194, 67-82. (doi:
 369 10.1016/S0012-821X(01)00553-2)
- 370 McKenzie, D., & O'Nions, R. K. (1991). Partial melt distribution from inversion of
 371 rare earth element concentrations. *Journal of Petrology*, 32, 1021-1091.
- 372 Miller, K. J., Zhu, W., Montésí, L. G. J., & Gaetani, G. A. (2014). Experimental
 373 quantification of permeability of partially molten mantle rock. *Earth and Plan-*
 374 *etary Science Letters*, 388, 273-282. (doi: 10.1016/j.epsl.2013.12.003)

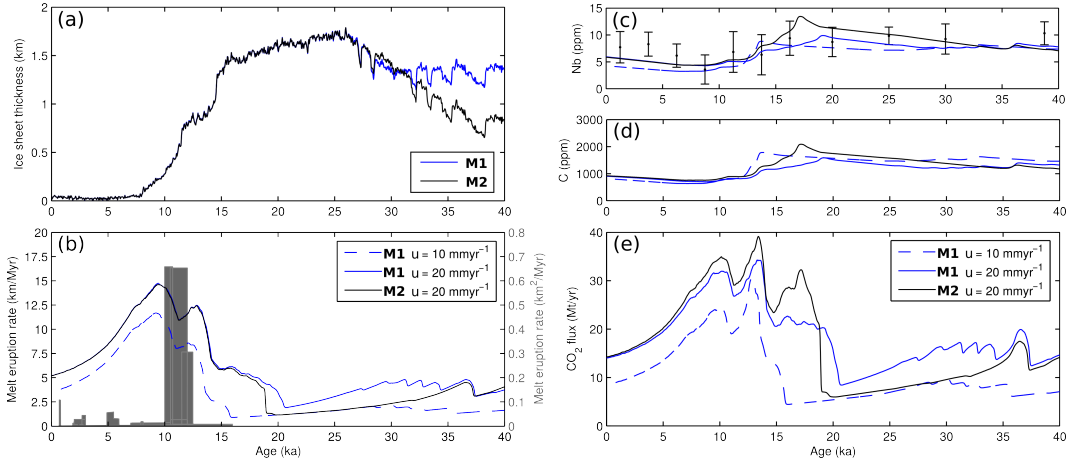
- 375 Nordahl, H., & Ingólfsson, O. (2015). Collapse of the Icelandic ice sheet controlled
 376 by sea level rise? *Arktos*, 1, 1-13. (doi: 10.1007/s41063-015-0020-x)
- 377 Patton, H., Hubbard, A., Bradwell, T., & Schomackere, A. (2017). The configura-
 378 tion, sensitivity and rapid retreat of the Late Weichselian Icelandic ice sheet.
 379 *Earth-Science Reviews*, 166, 223-245. (doi: 10.1016/j.earscirev.2017.02.001)
- 380 Peltier, W. R. (2004). Global glacial isostacy and the surface of the ice-age Earth:
 381 The ICE-5G (VM2) model and grace. *Annual Reviews of Earth and Planetary
 382 Science*, 32, 111-149. (2004)
- 383 Pico, T., Creveling, J. R., & Mitrovica, J. X. (2017). Sea-level records from the
 384 U.S. mid-Atlantic constrain Laurentide Ice Sheet extent during Marine Isotope
 385 Stage 3. *Nature Communications*, 8(15621). (doi: 10.1038/ncomms15612)
- 386 Rawson, H., Pyle, D. M., Mather, T. A., Smith, V. S., Fontjin, K., Lachowycz,
 387 S. M., & Naranjo, J. A. (2016). The magmatic and eruptive response of arc
 388 volcanoes to deglaciation: Insights from southern Chile. *Geology*, 44, 251-254.
 389 (doi: 10.1130/G37504.1)
- 390 Ribe, N. M. (1985). The generation and composition of partial melts in the earth's
 391 mantle. *Earth and Planetary Science Letters*, 73, 361-376.
- 392 Rosenthal, A., Hauri, E. H., & Hirschmann, M. M. (2015). Experimental determi-
 393 nation of C, F, and H partitioning between mantle minerals and carbonated
 394 basalt, CO₂/Ba and CO₂/Nb systematics of partial melting, and the CO₂
 395 contents of basaltic source regions. *Earth and Planetary Science Letters*, 415,
 396 77-87. (doi: 10.1016/j.epsl.2014.11.044)
- 397 Scott, D. R. (1992). Small-scale convection and mantle melting beneath mid-ocean
 398 ridges. In J. Phipps Morgan, D. K. Blackman, & J. M. Sinton (Eds.), *Mantle
 399 flow and melt generation at mid-ocean ridges* (Vol. Geophysical Monograph 71,
 400 p. 327-352). American Geophysical Union.
- 401 Shorttle, O., & MacLennan, J. (2011). Compositional trends of icelandic
 402 basalts: Implications for short-length scale lithological heterogeneity in
 403 mantle plumes. *Geochemistry Geophysics Geosystems*, 12, Q11008. (doi:
 404 10.1029/2011GC003748)
- 405 Sigvaldsson, G. E., Annertz, K., & Nilsson, M. (1992). Effect of glacier load-
 406 ing/delowering on volcanism: postglacial volcanic production rate of the Dyn-
 407 gjufjöll area, central Iceland. *Bulletin of Volcanology*, 54, 385-392. (doi:
 408 10.1007/BF00312320)
- 409 Silbeck, J. N. (1975). On the fluid dynamics of ridge crests. In *Notes on the 1975
 410 summer study program in geophysical fluid dynamics at the woods hole oceano-
 411 graphic institution*, (Vol. 2, p. 113-122).
- 412 Sinton, J., Grönvold, K., & Saemundsson, K. (2005). Postglacial eruptive history
 413 of the Western Volcanic Zone, Iceland. *Geochemistry Geophysics Geosystems*,
 414 6(Q12006). (doi: 10.1029/2005GC001021)
- 415 Sleep, N. H., & Snell, N. S. (1976). Thermal contraction and flexure of mid-
 416 continent and Atlantic marginal basins. *Geophysical Journal of the Royal
 417 Astronomical Society*, 45, 125-154.
- 418 Spiegelman, M. (1996). Geochemical consequences of melt transport in 2-D: The
 419 sensitivity of trace elements to mantle dynamics. *Earth and Planetary Science
 420 Letters*, 139, 115-132.
- 421 Spratt, R. M., & Lisiecki, L. E. (2016). A late Pleistocene sea level stack. *Climate of
 422 the Past*, 12, 1079-1092. (doi: 10.5194/cp-12-1079-2016)
- 423 Wasyljenki, L. E., Baker, M. B., Kent, A. J. R., & Stopler, E. M. (2003). Near-
 424 solidus melting of the shallow upper mantle: partial melting experiments on
 425 depleted peridotite. *Journal of Petrology*, 44, 116-1191.



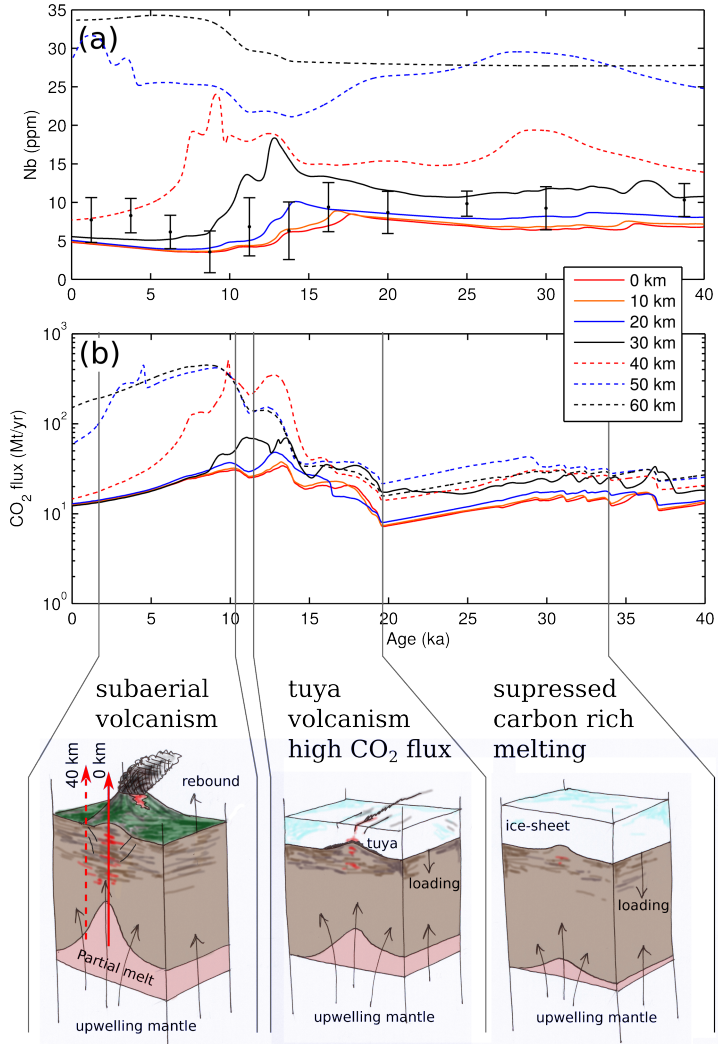
426 **Figure 1.** Profiles of porosity and S-wave seismic velocity for the two model permeabilities of
 427 $k_0 = 10^{-7} \text{ m}^2$ black line, and $k_0 = 10^{-5} \text{ m}^2$ red line. (a) Porosity plotted against depth at steady
 428 state. (b) S-wave velocity from the joint inversion of teleseismic and ambient noise Rayleigh
 429 waves (Harmon & Rychert, 2016) and the predicted S-wave profile from the high permeability
 430 case. The model includes the addition of the adiabatic gradient, the anharmonic effects from the
 431 mineralogy and effects of attenuation (Goes et al., 2012). The dashed line assumes melt has no
 432 effect, the solid line includes a 7.9 % reduction in V_S per percent melt (Hammond & Humphreys,
 433 2000). (c) S-wave velocity predictions for the low permeability case.



434 **Figure 2.** Response of the model to periodic and observed ice sheet thickness changes of the
 435 last 120 ka. (a) Map of Iceland showing the locations of the volcanic rift zones in orange and the
 436 maximum extent of the ice sheet at the last glacial maximum (dashed line). The boxes show the
 437 location of the Reykjanes Peninsular (R. P.) and the Western Volcanic Zone (W. V. Z.). (b) The
 438 ice sheet thickness predicted from the ice sheet model M1 over the last 120 ka. (c) Melt eruption
 439 rate and (d) carbon flux response to the step change in ice sheet thickness: black line, an upper
 440 mantle permeability coefficient of $k_0 = 10^{-5} \text{ m}^2$ and upwelling velocity of 10 mm yr^{-1} , and blue
 441 line, an upwelling velocity of 20 mm yr^{-1} .



442 **Figure 3.** Impact of ice sheet growth and decay on melt eruption and composition over the
 443 last 40 ka. (a) Ice sheet models M1 and M2 taken from the sea-level models of Peltier (2004) and
 444 Pico et al. (2017) respectively. (b) Melt eruption rates (in km of melt per Myr): blue solid line,
 445 ice sheet history 5G for $k_0 = 10^{-5} \text{ m}^2$ with an upwelling rate of 20 mm yr^{-1} ; blue dashed line, M1
 446 for $k_0 = 10^{-5} \text{ m}^2$ with an upwelling rate of 10 mm yr^{-1} ; black solid line, ice sheet history M2 for
 447 $k_0 = 10^{-5} \text{ m}^2$ with an upwelling rate of 20 mm yr^{-1} . The gray region shows estimated eruption
 448 rates from geological observations (MacLennan et al., 2002)] (in km^2 of melt per Myr). (c) Ob-
 449 served and predicted Nb concentrations (ppm), observations are from the Reykjanes Peninsula
 450 and the Western Volcanic Zone (Eason et al., 2015; Gee et al., 1998; Sinton et al., 2005) and are
 451 binned at 2.5 kyr intervals from 0 to 17.5 ka and then at 5 kyr intervals. (d) Predicted variation of
 452 in the concentration of carbon (ppm) within the erupted melt. (e) Predicted variation in the flux
 453 of CO_2 , assuming that the flux of CO_2 that Icelandic volcanism covers an area of $30,000 \text{ km}^2$, and
 454 $\text{CO}_2 (\text{ppm}) = 3.67 \text{ C (ppm)}$ (see Eq. 23 in the Supplementary Material).



455 **Figure 4.** Impact of glacial history on off-axis and on-axis melting. A series of 1D column
 456 melting models forced by the response to deglaciation (ice sheet history model M1) where the
 457 mantle flow is of steady state corner flow. (a) Nb concentrations from the centre of extension out
 458 to 60 km from the centre of extension. The mean concentration weighted by the eruption rate is
 459 plotted as the thick black line. (b) Predicted CO₂ flux from the series of vertical melting models.
 460 The late-Pleistocene eruptions are typified by tuya magmatism. This will have been the case up
 461 until at least ~14 ka, where either magmatism was suppressed or when eruptions occurred they
 462 will have been beneath at least 1 km of ice-cover (Hartley et al., 2016). The suppressed melting
 463 regime will have become carbon rich because the shallow low-C melt production is damped due
 464 to the ice-sheet loading. Upon deglaciation there is increased volcanism, which initially taps the
 465 melt rich carbon.